analytical chemistry

Article

pubs.acs.org/ac

Argon Cluster Ion Beams for Organic Depth Profiling: Results from a VAMAS Interlaboratory Study

Alexander G. Shard,*[,†] Rasmus Havelund,[†] Martin P. Seah,[†] Steve J. Spencer,[†] Ian S. Gilmore,[†] Nicholas Winograd,[‡] Dan Mao,[‡] Takuya Miyayama,[§] Ewald Niehuis,[▽] Derk Rading,[▽] and Rudolf Moellers[▽]

[†]National Physical Laboratory, Teddington, Middlesex, TW11 0LW, United Kingdom

[‡]Department of Chemistry, Pennsylvania State University, 104 Chemistry Building, University Park, Pennsylvania 16802, United States

[§]ULVAC-PHI, Inc., 370 Enzo, Chigasaki, 253-8522, Japan

[▽]ION-TOF GmbH, Heisenbergstr. 15, D-48149 Muenster, Germany

ABSTRACT: The depth profiling of organic materials with argon cluster ion sputtering has recently become widely available with several manufacturers of surface analytical instrumentation producing sources suitable for surface analysis. In this work, we assess the performance of argon cluster sources in an interlaboratory study under the auspices of VAMAS (Versailles Project on Advanced Materials and Standards). The results are compared to a previous study that focused on C_{60}^{q+} cluster sources using similar reference materials. Four laboratories participated using time-of-flight secondary-ion mass spectrometry for analysis, three of them using argon cluster sputtering sources and one using a C_{60}^{+} cluster source. The samples used for the study were organic multilayer reference materials consisting of a ~400-nm-thick Irganox 1010 matrix with ~1 nm marker layers of Irganox 3114 at depths of ~50, 100, 200, and 300 nm. In accordance with a previous report, argon cluster sputtering is shown to provide effectively constant sputtering yields through these reference materials. The work additionally demonstrates that molecular secondary ions may be used to monitor the depth profile and depth resolutions approaching a full width at half maximum (fwhm) of 5 nm can be achieved. The participants employed energies of 2.5 and 5 keV for the argon clusters, and both the sputtering yields and depth resolutions are similar to those extrapolated from C_{60}^{+} cluster sputtering data. In contrast to C_{60}^{+} cluster sputtering, however, a negligible variation in sputtering yield with depth was observed and the repeatability of the sputtering yields obtained by two participants was better than 1%. We observe that, with argon cluster sputtering, the position of the marker layers may change by up to 3 nm, depending on which secondary ion is used to monitor the material in these layers, which is an effect not previously visible with C_{60}^{+} cluster sputtering. We also note that electron irradiation, used for charge compensation, can induce molecular damage to areas of the reference samples well beyond the analyzed region that significantly affects molecular secondary-ion intensities in the initial stages of a depth profile in these materials.

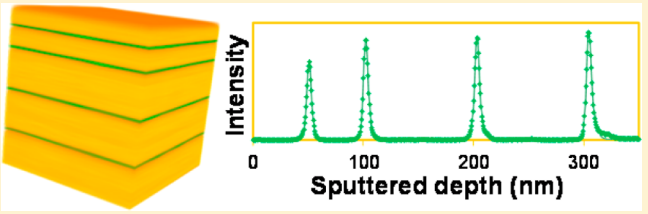

Cluster ion beams, in combination with a surface-sensitive analytical technique such as X-ray photoelectron spectroscopy (XPS) or secondary-ion mass spectrometry (SIMS), have been shown to provide the ability to depth profile organic materials while retaining molecular information. In contrast to atomic ions, cluster ions do not penetrate deeply into target materials and, therefore, the energy of their impact is deposited within the first few nanometers of the surface, resulting in high sputtering yields and minimal subsurface damage.[1] This discovery offers the potential for analysts to measure the distribution of organic materials through micrometers of industrially and medically relevant materials with depth resolutions in the region of 10 nm.[2−11] There are few, if any, analytical methods that can rival this level of detail without either special preparation of the sample or labeling of the components of interest with detectable functional groups, elements, or isotopes. In the past decade, the community of SIMS practitioners and instrument manufacturers has acquired an understanding of the underlying processes[12−17] and the key experimental parameters[18−22] that lead to the best analytical performance.

For many years, the main barrier to progress in the improvement of cluster-ion-beam depth profiling was the lack of a means to compare performance. This issue is best addressed using a reference sample with a known composition and structure. Ideally, the reference sample should have sharp interfaces between layers of materials at known depths so that sputtering yields and depth resolutions can be easily found.

Received: June 7, 2012
Accepted: August 16, 2012
Published: August 16, 2012

   dx.doi.org/10.1021/ac301567t | *Anal. Chem.* 2012, 84, 7865−7873

Examples of such materials include spin-cast polymers,[23] Langmuir–Blodgett films,[24] and vacuum-evaporated layers.[25] The latter method has been shown to produce useful and stable reference materials with the capacity for batch production and excellent reproducibility. Such reference materials also provide valuable data through which theoretical understanding, such as that provided by molecular dynamics (MD) simulations, can be tested and validated.[26] In a VAMAS (Versailles Project on Advanced Materials and Standards) interlaboratory study, carried out in 2009, alternating vacuum evaporated layers of Irganox 1010 and Irganox 3114 were used to establish the repeatability and reproducibility of organic depth profiling.[27,28] That study demonstrated that cluster-ion-beam sputtering can provide results with a repeatability (relative standard deviation, RSD) of better than 5%, and that the comparability between laboratories was also excellent, in terms of sputtering yield and depth resolution.

Of equal importance in the study was the opportunity provided for participants to validate experimental approaches to depth profiling with cluster ion beams which had previously been suggested, such as sample rotation,[20,29] sample cooling,[17,20] different angles of irradiation,[30,31] and the creation of bevels for retrospective analysis.[32,33] At the time of the 2009 VAMAS interlaboratory study, most analysts were using C_{60}^{q+} ions as the sputtering species; none of the participants employed argon cluster sources (Ar_n^+, with n typically larger than 500). However, based upon the realization that argon cluster sources can provide constant sputtering yields through a wider variety of materials,[11,34] an increasing emphasis has been placed on these as a sputtering source. A study of the VAMAS materials on a prototype instrument revealed that Ar_n^+ ion sputtering could provide a constant sputtering rate at a depth of over 400 nm,[35] without any of the special conditions, such as sample cooling, rotation, or low angle sputtering, which C_{60}^{q+} ions require to achieve the same result. Subsequently, many instrument manufacturers have developed argon cluster ion sources specifically for depth profiling. These are smaller than the prototype system, similar in size to traditional sputtering sources, and enable an even dose to be applied to the analysis area. To benchmark the performance of these new cluster sources, a second VAMAS study on organic depth profiling was initiated by NPL, using materials similar to those in the first study. The results of this second study are reported in this article.

EXPERIMENTAL SECTION

Organic multilayer reference materials were constructed from Irganox 1010 and Irganox 3114 (CIBA, Macclesfield, U.K.), using a procedure described previously.[28] In brief, silicon wafers were coated with five layers of Irganox 1010 interspersed with four layers of Irganox 3114 by thermal evaporation in an Edwards AUTO306 vacuum coater. The Irganox 3114 layers were ∼1 nm thick and spaced at depths of ∼50 nm, ∼100 nm, ∼200 nm, and ∼300 nm beneath the surface of the complete multilayer. The complete multilayer film was ∼400 nm thick. A schematic of the samples used in the study is shown in Figure 1. The thickness of each layer was monitored by a quartz crystal microbalance, which had previously been calibrated to the thickness measured by spectroscopic ellipsometry (M2000DI, Woollam, NE, USA) on pure layers of each material prepared immediately before the construction of reference materials. Using a well-established relationship between deposited thickness, the QCM measurement, the position of the evaporation source, and the position of the sample, individual layer thicknesses on each sample could be calculated to within 4% error. The materials used in this study differed from those used in the previous VAMAS study[28] importantly, in that the Irganox 3114 layers were thinner. This reduction was to accommodate the possibility that the original 3 nm width would contribute to the observed depth resolution.

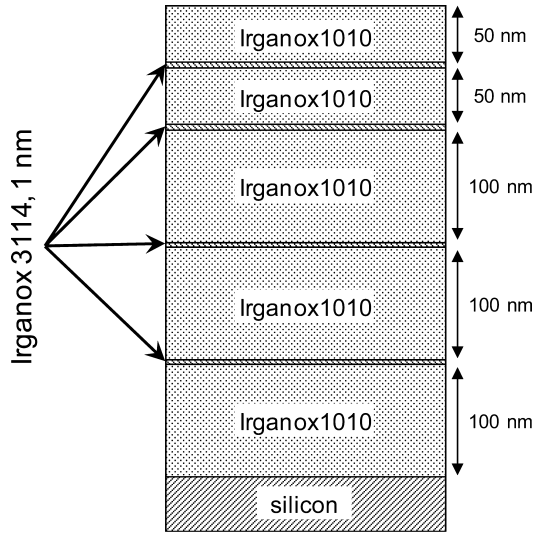

Figure 1. Schematic of the structure of the multilayered samples used in this study. Thicknesses shown here are nominal, the thicknesses of each organic layer on each sample are known precisely.

All participants recorded depth profiles from a single batch of material OML09, except for participant B, who also analyzed a second batch, OML14 which was made at a later date to clarify the cause of some minor issues that became evident in the first batch, as explained later.

Samples were sent to the participating institutions and analysis was performed on four separate instruments, only two of which had the same manufacturer and three of which were equipped with argon cluster ion sources and one equipped with a C_{60}^+ ion source. The inclusion of the latter was helpful to ensure that comparable results were obtained with the previous VAMAS investigation. All participants employed time-of-flight secondary-ion mass spectrometry (ToF-SIMS) for analysis of the sputtered surface. A summary of the sputtering and analytical sources used by participants on their separate instruments are provided in Table 1. All participants recorded beam currents before and after each experiment. They performed a sequential sputtering and analysis cycle using a sputtered area with lateral dimensions more than twice the analysis area to ensure an even sputtering ion dose across the analysis area. The participants recorded the negative secondary-ion intensities of six species related to the matrix material, Irganox 1010, namely, C_2HO^- (m/z = 41.003 Da); $C_2H_3O_2^-$ (59.013 Da); $C_{12}H_{15}O^-$ (175.112 Da); $C_{16}H_{23}O^-$ (231.175 Da); $C_{17}H_{25}O_3^-$ (277.180 Da), and the deprotonated molecular secondary ion $C_{73}H_{107}O_{12}^-$ (1175.776 Da). The $C_{73}H_{107}O_{12}^-$ ion is termed $[M_{1010}-H]^-$ for convenience. Secondary ions arising from the marker layer material, Irganox 3114, were also recorded: CN^- (26.003 Da); CNO^- (42.001 Da); $C_{18}H_{24}N_3O_4^-$ (346.117 Da) and $C_{33}H_{46}N_3O_5^-$ (564.344 Da). The $C_{33}H_{46}N_3O_5^-$ ion is termed $[M_{3114}-R]^-$ for convenience. Note that, for Irganox 3114, the deprotonated secondary ion $C_{48}H_{68}N_3O_6^-$ (782.510 Da) is not observed,

dx.doi.org/10.1021/ac301567t | Anal. Chem. 2012, 84, 7865–7873

Table 1. List of Sputtering Ion Sources and Analysis Ion Sources Used by Participants in This Study, Experimental Conditions Are Also Listed

participant	batch	sputtering source, energy, angle from sample normal	analysis source energy, angle from sample normal	ratio of analysis dose to sputtering dose	sample conditions
A	OML09	C_{60}^+, 40 keV, 40°	C_{60}^+, 40 keV, 40°	0.0033	cooling (90 K), no rotation
B0	OML09	Ar_{2000}^+, 5 keV, 45°	Bi_3^+, 13 keV, 45°	0.0009	room temperature, no rotation
C	OML09	Ar_{2500}^+, 2.5 keV, 40°	Bi_3^{+2}, 60 keV, 40°	0.00018	room temperature, sample rotation at 0.5 rpm
D	OML09	Ar_{1700}^+, 2.5 keV, 45°	Bi_3^+, 15 keV, 45°	0.0006	room temperature, no rotation
B1	OML14	Ar_{2000}^+, 5 keV, 45°	Bi_3^+, 25 keV, 45°	0.0009	room temperature, no rotation
B2	OML14	Ar_{2000}^+, 5 keV, 45°	Bi_3^+, 25 keV, 45°	0.0039	room temperature, no rotation

presumably because of the lability of the R═$C_{15}H_{23}O$ "arms" that surround the central cyanurate ring of this molecule. The participants returned the analytical data in the form of ion intensity versus sputtering time to NPL for further analysis. Dose rates were calculated from the quotients of the sputtering beam currents, and the sputtered areas are provided by the participants.

RESULTS AND DISCUSSION

In Figure 2, a comparison is made between the results from the four different laboratories, plotting the $[M_{3114}-R]^-$ secondary-ion intensities against dose. All four participants were able to profile the reference materials and resolve all of the marker layers using all of the secondary ions that uniquely arise from the marker layer material. As shown by the solid lines in Figure 2, the intensity versus dose curves for each layer are well-described by the response function given by Dowsett.[36] There are some deviations from this function in the tail of the third and fourth layers, which are evident in the data from participants B0, C and D. An investigation into the cause of these features revealed that the most likely cause was cross contamination of Irganox 3114 onto the Irganox 1010 crucible. The installation of a screen between the two crucibles was sufficient to eliminate this problem, as shown by the data from a later batch of samples in Figure 2 for participant B1, where the curves are well-described by the Dowsett response function over the full range of intensities (approaching 3 orders of magnitude, not shown in this plot). This feature of the original batch of samples illustrates how SIMS depth profiling with this depth resolution can measure *genuine* detailed structure. Here, these features do not affect the measured depth resolutions for the first three layers and do not affect any of the marker layer positions.

All of the participants were able to achieve a constant sputtering yield from the first to the last Irganox 3114 layer. This was established by plotting the known central depths of each layer against the dose required to obtain the relevant maximum in the $[M_{3114}-R]^-$ secondary-ion intensity. In the case of a constant sputtering yield, this plot should yield a straight line, and indeed does, as shown in Figure 3, the slope of which is the sputtering yield volume, i.e., the average volume of material removed by each impact. Unconstrained linear regression also provides the zero dose intercept, which provides some information with regard to either the nature of the sample surface or the assumption of constant sputtering yield in the near-surface region. Results from participants are expressed as sputtering yield volume (slope) and depth offset (intercept) and are listed in Table 2. It is notable that participants B and D, who used argon cluster sources and provided repeat data, had excellent repeatability (better than 0.5% variation) in sputtering yields. This compares to a typical 5% RSD for C_{60}^{q+} sputtering in the previous VAMAS study, which is consistent with the results from participant A.

Participant B provided two sets of data (B1 and B2) using different ratios of analysis beam to sputtering beam doses for sample OML14. The change in dose rate in the two cases has been estimated both from the times to the peaks in the profiles and the total secondary-ion intensities obtained. The ratio of Bi_3^+ dose rate (analysis) to Ar_{2000}^+ dose rate (sputtering) changed from ∼0.09% in B1 to ∼0.39% in B2, and although these values are uncertain, because of the low accuracy in measuring the small (∼0.1 pA) analysis beam currents, the change in the ratios by a factor of 4.2 is more certain. If it is assumed that the sputtering and analysis beams contribute additively to the total sputtering yield and there are no additional effects from the electron-beam-induced damage discussed later, an estimate that the sputtering yield from 5 keV Ar_{2000}^+ alone is 32.3 nm^3 per incident ion can be made using a method similar to that used by Brison et al. in a study of dual-beam sputtering with C_{60}^+ ions of tetraglyme plasma polymers.[37] In that work, Brison et al. employed much higher ratios of analysis to sputtering dose rates to observe significant effects; however, their approach may be of greater importance with argon cluster sputtering, because of the higher accuracy that may be acquired, compared to C_{60}^+ sources and the lower ion energies and sputtering yields, which are used to improve depth resolution. Both of these factors mean that the contribution of the analysis beam to the total sputtering rate is observable under normal experimental conditions and, in work where accuracy is important, may be significant.

For participants A and D, the variability in the depth offset is explicable from the variability found for the sputtering yield and is consistent with a negligible change in sputtering yield in the top 50 nm of the sample. On their OML09 samples, participants B and D obtained a similar depth offset of ∼1 nm. Participant B found a consistently negative depth offset for their data returned in this study on sample OML14, which should arise from one or more of three effects: (i) the top layer of this batch was thicker than expected; (ii) the surface had a layer of contamination; and/or (iii) the sputtering yield in the top 50 nm was, on average, lower than the remainder of the sample. An additional feature of these data is that the variability in the depth offset is larger than would be expected from the variability in sputtering yields, showing that the effect is not constant from profile to profile. The SIMS spectra reconstructed from the top layer of this sample did not show any identifiable contaminants and were consistent with damaged Irganox 1010, as demonstrated later. We note that a negative offset appears to be correlated with a transient rise in matrix signal discussed later, which may be due to sample

dx.doi.org/10.1021/ac301567t | Anal. Chem. 2012, 84, 7865−7873

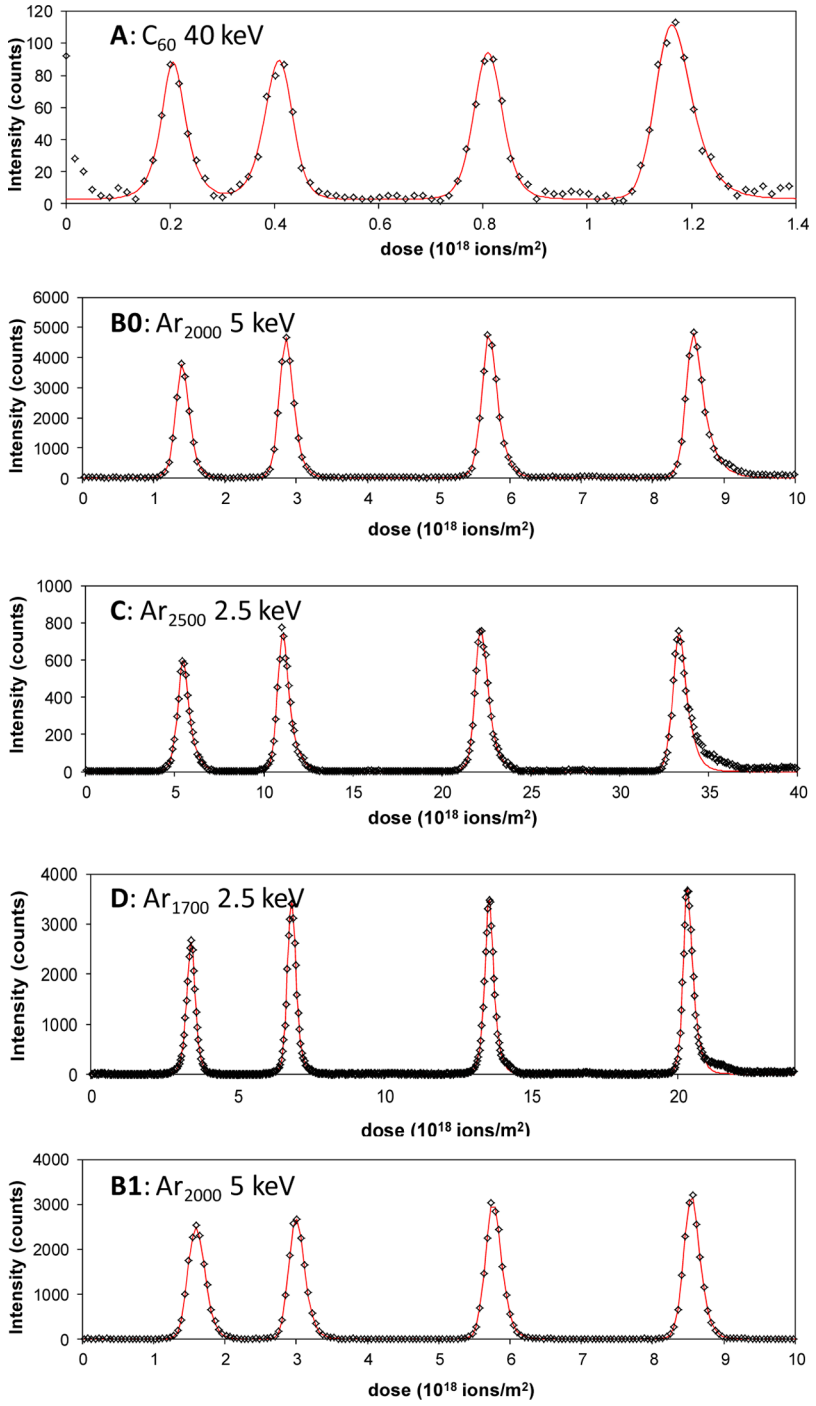

Figure 2. Results from the four participants, plotting the $[M_{3114}-R]^-$ secondary-ion intensities against sputtering ion dose. Data points show the raw data and lines connect points in a fit to the data using Dowsett's response function. The participant code, sputtering source, and energy are shown in the top left corner of each graph. Dataset B1 used a sample from a later batch.

damage, and further work is required to understand the origin of this effect.

The depth resolution for each layer is expressed as the full width at half-maximum (fwhm) and calculated from the Dowsett response function fitted to the data. Table 2 lists the mean depth resolution and standard deviation achieved by each participant. Only the first three layers were included, to avoid any material-dependent broadening associated with the distinct feature on the last layer. Participant D achieved a remarkable fwhm depth resolution of 5 nm over these three layers. Participant C used rotation, which can potentially degrade depth resolution, however the rotation rate (one complete cycle every 30 s) was much longer than the time to complete a raster frame (~0.13 s); therefore, the regional variation in sputtering dose caused by the use of raster and rotation was negligible.[38] The higher variability in depth resolution shown by participants A and B2 arise from reproducible changes in the fwhm of the signals arising from different layers. For participant A, the first layer was narrower (fwhm ≈ 13.4) than the second and third layers (~15.7 nm), and for participant B2, the third layer was narrower (~6.4 nm) than the first two (~9.3 nm); this was not observed in the first (B1) dataset on the same

dx.doi.org/10.1021/ac301567t | Anal. Chem. 2012, 84, 7865−7873

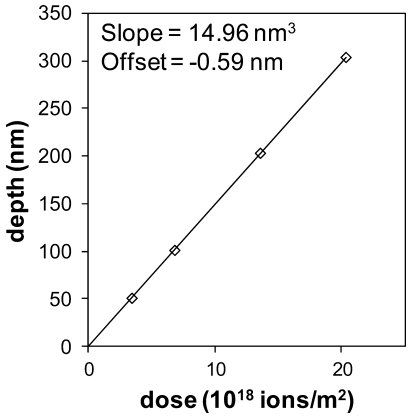

Figure 3. Example plot of the known central depth of each layer against the sputtering dose required to reach a maximum $[M_{3114}-R]^-$ secondary-ion intensity for one profile provided by participant D. Linear regression provides the sputtering yield volume as the slope and a depth offset, negative values for offset imply that the marker layers are reached later than expected. The data scatter around the fit by <0.1 nm.

Table 2. Sputtering Yield Volumes, Depth Offsets and Depth Resolutions from the First Three Layers Obtained from Analysis of $[M_{3114}-R]^-$ Secondary-Ion Intensities (see Figures 2 and 3)[a]

participant	number of datasets	sputtering yield volume (nm^3)	depth offset (nm)	depth resolution, fwhm (nm)
		Reference Material OML09		
A	2	247.5 ± 13	+0.3 ± 3.2	14.9 ± 1.3
B0	1	34.10	+1.2	7.8 ± 0.6
C	1	8.94	+1.1	6.9 ± 0.6
D	2	14.93 ± 0.04	−0.3 ± 0.3	5.1 ± 0.1
		Reference Material OML14		
B1	3	32.89 ± 0.04	−8.0 ± 1.0	9.0 ± 0.3
B2	2	34.69 ± 0.11	−9.8 ± 3.2	8.3 ± 1.6

[a]When repeat measurements have been provided, the number of profiles and range of results are also described.

sample and the reason for this result is unclear. Participants C and D employed the same energy of cluster ions for sputtering, but observed rather different depth resolutions. The difference in cluster size may account for this observation, but it is more likely that the contribution from the information depth of the analytical beam is responsible. Participant C used 60 keV Bi_3^{2+} and participant D used 15 keV Bi_3^+, which is a factor-of-4 difference in energy with an ∼2 nm difference in depth resolution. Muramoto et al.[22] reported an information depth increase for organic materials of ∼1 nm on changing analysis beam energies by a factor of 2 from 25 keV Bi_3^+ to 50 keV Bi_3^{2+}.

In the previous VAMAS study on organic depth profiling, empirical relationships between C_{60}^{q+} energy, sputtering yield, and depth resolution were established.[28] These were valid for impact angles of ∼45° and for samples at room temperature. Samples that were cooled demonstrated a decrease in sputtering yield to ∼75% of the room temperature value at an impact energy of 10 keV.[20] In Figure 4, the results of this study are compared to the previous VAMAS study and very similar behavior was found. It should be noted that the argon cluster energies used in this study are lower than those for C_{60}^{q+} in the previous study, where the lowest energy was 10 keV. Even so, Figure 4a shows that the sputtering yields are comparable as previous reports have indicated,[35,39] although Ar cluster size as well as energy can also strongly affect sputtering yields.[40] For C_{60}^+ at 40 keV with the sample at 90 K, the sputtering yield is ∼80% of that expected for a sample at room temperature, and this is consistent with previous data, as described above. The correlation between depth resolution and sputtered volume per incident ion is also similar to the previous VAMAS study, as shown in Figure 4b; the scatter shown here is also similar to that of previous data. The important result of this plot is to demonstrate that Ar_n^+ ions provide better depth resolution than C_{60}^{q+} ions, primarily because they are able to sputter organic materials with a lower incidence energy and, hence, a smaller sputtering yield with concomitant smaller crater size. Sputtering organic materials at 5 keV with C_{60}^+ is problematic,[25] and there are no literature reports of successful depth profiles at 2.5 keV.

The analysis provided above has concentrated on the results from the $[M_{3114}-R]^-$ secondary-ion intensities, the same analysis was also applied to the CN^- (26.003 Da), CNO^- (42.001 Da), and $C_{18}H_{24}N_3O_4^-$ (346.117 Da) secondary-ion intensities. These also uniquely arise from the Irganox 3114 marker layers. An interesting observation is that, although the analysis produced identical sputtering yields to those obtained from $[M_{3114}-R]^-$ secondary ions, the depth offsets were different. In particular, the CNO^- secondary-ion consistently appeared earlier in the profile than the $[M_{3114}-R]^-$ secondary

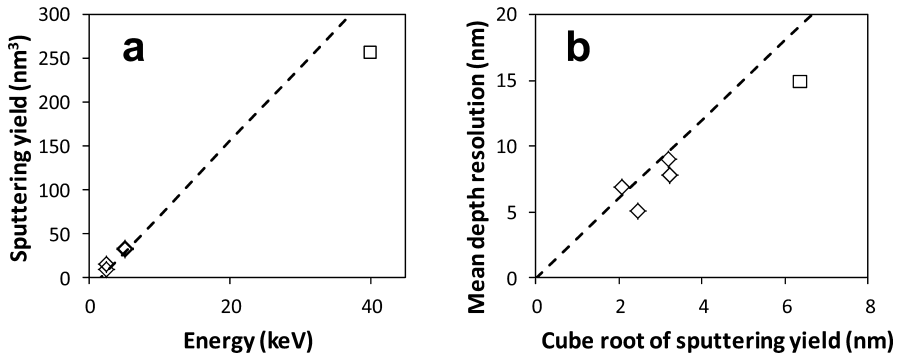

Figure 4. Comparison of the results of this VAMAS study to C_{60}^{q+} results from the previous VAMAS study: (a) sputtering yield plotted against sputtering species energy, (b) mean depth resolution plotted against the cube root of the sputtering yield. Legend: (◇) Ar_x^+ results from participants B1, C, and D; and (□) C_{60}^+ at 90 K from participant A. Dashed lines show the relationships established for C_{60}^{q+} in the previous VAMAS investigation.

dx.doi.org/10.1021/ac301567t | Anal. Chem. 2012, 84, 7865−7873

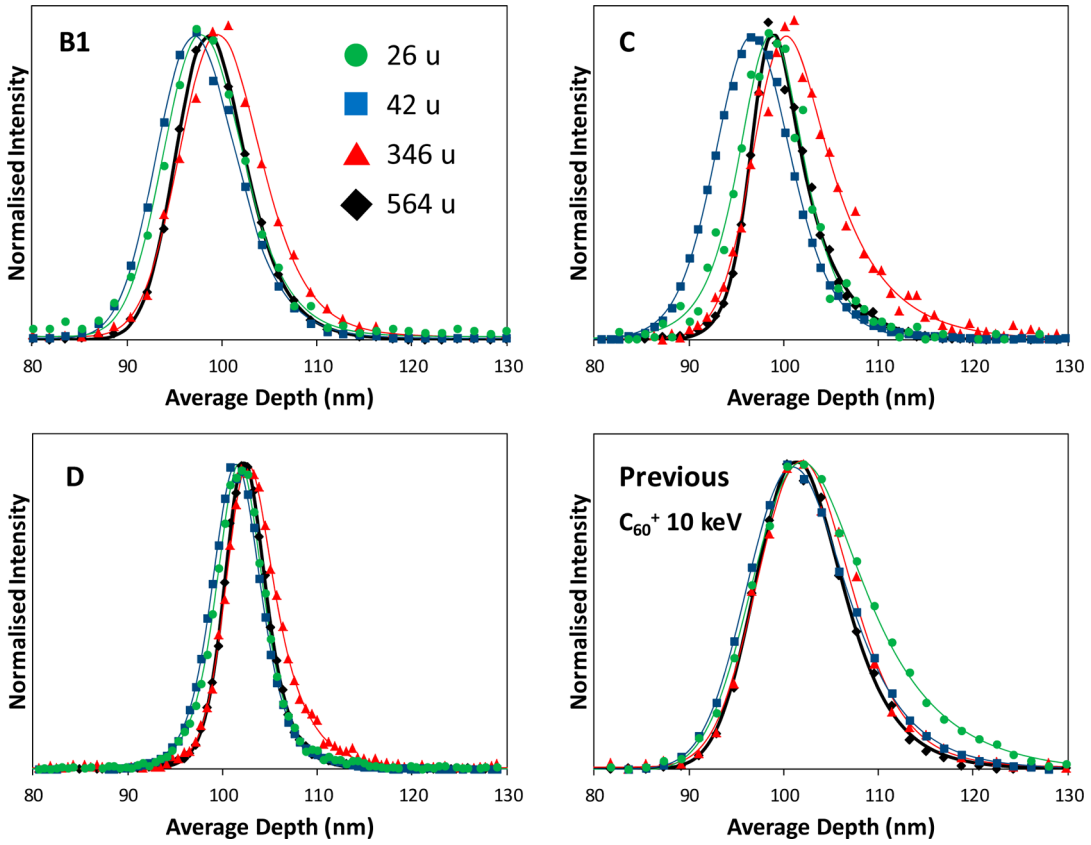

Figure 5. Graphs showing the difference between secondary ions that may be used to identify the positions of Irganox 3114 marker layers; examples are from the second (~100 nm deep) layer. Markers show the experimental secondary-ion intensities: green circles represent data for CN^- (26.003 Da); blue squares represent data for CNO^- (42.001 Da); red triangles represent data for $C_{18}H_{24}N_3O_4^-$ (346.117 Da); and black diamonds represent data for $[M_{3114}-R]^-$ (564.344 Da). Solid lines are fits to the data using Dowsett's response function and intensities are normalized so that the maximum value of the fitted curves are identical. Data are shown from three participants using argon cluster sources (B1, C, and D) and, for comparison, data for C_{60}^+ from the previous VAMAS study.[28]

ion for argon cluster sputtering. These effects are shown in Figure 5, where it is clear that both of the light ions, CN^- and CNO^-, have response curves that rise in advance of the $[M_{3114}-R]^-$ response curve. The effect is most pronounced for the CNO^- secondary ion in which the onset (taken as the point to reach 50% of the maximum intensity) is ~2 nm for participant B1, ~4 nm for C, and ~1 nm for D and B0. Data from participant A, who used C_{60}^+, did not show these effects, although the depth resolution in their case means that the result is not as clear as some of the results from the previous VAMAS study.[28] In Figure 5, an example is shown from that previous dataset with depth resolution approaching that of B1 (C_{60}^+, 10 keV, −80 °C) and using an identical analytical ion source to B1, where the effect is clearly not as pronounced. Also evident is the extended tail to increasing depth for the $C_{18}H_{24}N_3O_4^-$ secondary ion during argon cluster sputtering, which does not occur with C_{60}^+ sputtering, as is clear in Figure 5. For C_{60}^+ sputtering there is, instead, an extended tail for the CN^- secondary ion. In all cases, the $[M_{3114}-R]^-$ secondary ion provides the narrowest response function and, therefore, the best depth resolution. Since participants B, C, and D used different sputtering rates and sputtering and analysis sources, it is not possible to determine which of these parameters influences this offset between the profiles for the different secondary ions. Potential causes are (i) different information depths for different secondary ions, (ii) mixing during sputtering, (iii) matrix effects in the ion emission process, and/or (iv) diffusion or surface segregation of species generated during the sputtering or analysis process. This phenomenon bears further investigation, because it affects the uncertainty in determining the identity, position, and width of layers and interfaces in organic depth profiling with argon cluster sources.

A significant concern raised in the study was the observation of transient variations at the start of some of the profiles in the intensities of secondary ions. In Figures 6a and 6b, the intensities from the $[M_{1010}-H]^-$ (1175.776 Da) and $C_{17}H_{25}O_3^-$ (277.180 Da) secondary ions are compared. Participant C provided data in which no significant transient was evident in these profiles, or those from other Irganox 1010-related secondary ions. Both participants B and D demonstrated transient behavior, with ion intensities increasing with depth into the sample; in the case of participant B, this transient behavior extended over many tens of nanometers. This is in contrast to C_{60}^+ sputtering under similar conditions, as shown from the traces from the same data set shown in Figure 5 from the previous VAMAS study. The secondary-ion intensities in Figures 6a and 6b are normalized to the signal at a depth of 150 nm to emphasize transient changes. This presentation should not be interpreted to indicate that, in C_{60}^+ sputtering, the initial secondary-ion intensity is higher than during argon cluster profiling. In fact, the secondary-ion intensities at a depth of 150 nm in the argon cluster profiles are similar to the *initial* intensities in C_{60}^+ profile for similar instruments. In the C_{60}^+ case, the transient decline in

dx.doi.org/10.1021/ac301567t | *Anal. Chem.* 2012, 84, 7865−7873

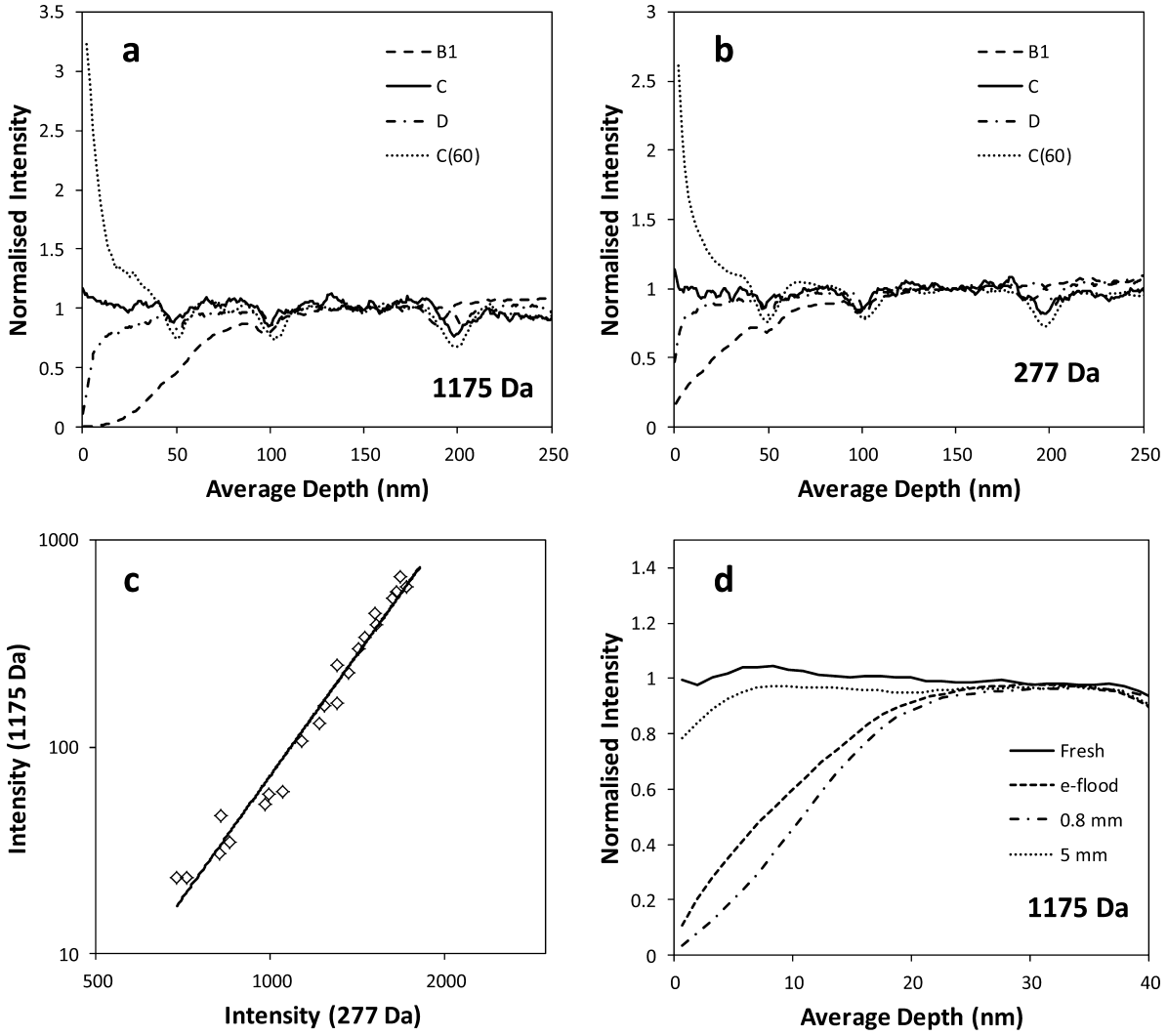

Figure 6. (a and b) Results from three participants from this study and one from a previous VAMAS study, plotting secondary-ion intensities from the Irganox 1010 matrix against average depth. Data are smoothed with a five-point running average and normalized to the intensity at an average depth of 150 nm. (c) Log–log plot of the $[M_{1010}–H]^-$ (1175.776 Da) secondary-ion intensities against those of $C_{17}H_{25}O_3^-$ (277.180 Da) from the initial 40 nm rise in intensity for B1. The power-law fit has an index of 3.9. (d) Additional datasets from participant B, presented as in panel (a) but expanded near the origin, on a sample without any previous flood gun exposure (fresh), after electron flood gun exposure (e-flood), and after two subsequent profiles (one 0.8 mm and the other more than 5 mm away from the "e-flood" position).

secondary-ion intensity can be understood in terms of damage induced by the sputtering ion beam.[12] The transient increase observed for argon cluster beams, on the other hand, is consistent with the removal of molecular damage as the sputtering proceeds; this is evident from the approximately fourth-power relationship observed between the $[M_{1010}–H]^-$ (1175.776 Da) and $C_{17}H_{25}O_3^-$ (277.180 Da) secondary-ion intensities shown in Figure 6c for participant B1. The smaller ion is essentially one of four identical "arms" of the complete Irganox 1010 molecule and the probability of finding an intact molecule is equal to the product of the probability of finding each component part of the molecule intact, as has been shown previously for poly(lactide).[13] Therefore, as long as the ratio of the two secondary-ion yields remains constant, damage effects should produce a fourth-power relationship between these two ion intensities. One should note that a transient rise may also be explained by a contaminant overlayer, but the relationship shown in Figure 6c would not be expected. In the case of participant B, it appears that molecular damage is the most probable cause; however, for participant D, the relationship is closer to third power and other factors, such as contaminants, may influence this transient rise. However, participant D could not identify any contaminant from their SIMS spectra.

The damage is not intrinsic to the samples themselves, since it is not observed in all profiles, but is most likely caused prior to analysis through either storage and handling by participants, or electron-beam irradiation from the flood gun used for surface charge stabilization during preparation for profiling, or from previous profiles. With respect to storage, excessive light exposure, for example, is known to damage these materials and they are always packaged and shipped in foil for this reason. The effect of electron-beam damage was shown in a separate experiment by participant B, the results of which are given in Figure 6d. Participant B used a 20 eV electron-beam current of 10 μA with a beam diameter of 2.6 mm on the sample. Four profiles are shown: in one, all preparation of the instrument was performed before moving the sample into the analysis position, this profile is labeled "fresh" and shows no significant transient; the second profile was performed after deliberate exposure to electron flood gun irradiation with $\sim 2 \times 10^{22}$ electrons/m^2

dx.doi.org/10.1021/ac301567t | *Anal. Chem.* 2012, 84, 7865–7873

(2000 s of the above beam), this profile is labeled "e-flood"' and shows damage effects; the third and fourth profiles were taken close to (0.8 mm and ~3×10^{22} electrons/m^2) and far from (>5 mm) the e-flood profile and demonstrate both the cumulative effects of electron beam damage and the necessity to perform repeat measurements a significant distance (greater than the radius of the electron beam spot on the sample, in this case, 1.3 mm) away from a previous profile to minimize these effects. It should be noted that the above doses are far in excess of the recommended limit[41] of 6×10^{18} electrons/m^2 for static SIMS, but also that the doses required for charge neutralization of the higher beam currents used in depth profiling experiments are necessarily larger than those for surface spectroscopy.

These results highlight the care needed in using electron flood guns for SIMS of sensitive organic materials, for which the difficulties are well-understood and guidance has previously been given for static analysis.[41] The present study shows that electron-induced damage of organic materials can affect the initial stages of an organic depth profile and additional guidance on the use of electron flood guns may be required to minimize these effects, because of the large electron doses employed during a profile and the necessity in some cases to perform repeat profiles in close proximity to previous ones. This issue has been of less importance in C_{60}^{q+} sputtering of organic materials, because charge compensation using electrons often was not necessary.[25,42]

CONCLUSIONS

This VAMAS (Versailles Project on Advanced Materials and Standards) study has demonstrated the capability of Ar_n^+ ions to depth-profile multilayered organic reference materials using time-of-flight secondary-ion microscopy spectroscopy (ToF-SIMS) analysis to detect molecular species. These ions achieve a depth resolution significantly better than C_{60}^{q+} ions, and the primary reason seems to be the lower beam energies that may be used with argon clusters. In addition, the depth resolution and sputtering yield for argon clusters remains constant throughout the profile, which is rarely the case for C_{60}^{q+}. The participants in this study who used argon clusters and provided several repeat profiles achieved an ~10-fold improvement in repeatability in sputtering yield, compared to C_{60}^{q+} sputtering in the previous VAMAS study. This is a testament to the stability of at least some of the argon cluster sources employed in this study. We observe that the position of the Irganox 3114 layers in the reference material may be altered by several nanometers, depending on the secondary ion that is used to identify them. This effect varies rather widely between participants, and the origin of this effect will be investigated.

Argon cluster sputtering is capable of providing depth profiles without transient changes in secondary-ion intensity during the initial stages of the profile for these materials. This indicates an essentially damage-free sputtering process. However, two of the participants provided data with significant surface transients where the secondary-ion intensities rose during the initial stages of the profile. This effect is likely to be caused by damage induced prior to the profiling experiment. In one case, this was sufficient to remove any trace of the $[M_{1010}\text{-}H]^-$ secondary-ion signal from the surface of the material, indicating complete destruction of all Irganox 1010 molecules. The study also highlights the care that is required to reduce or eliminate electron-beam damage if molecular identification is required within the first 10 nm or so of the surface.

AUTHOR INFORMATION

Corresponding Author

*E-mail: alex.shard@npl.co.uk.

Notes

The authors declare no competing financial interest.

ACKNOWLEDGMENTS

This work forms part of the Chemical and Biological Programme of the National Measurement System of the UK Department of Business, Innovation and Skills (BIS). We thank Steve A. Smith from NPL for assisting in the production of the samples used in this study.

REFERENCES

(1) Gillen, G.; Roberson, S. *Rapid Commun. Mass Spectrom.* **1998**, *12*, 1303−1312.
(2) Mahoney, C. M.; Fahey, A. J. *Anal. Chem.* **2008**, *80*, 624−632.
(3) Fletcher, J. S.; Conlan, X. A.; Lockyer, N. P.; Vickerman, J. C. *Appl. Surf. Sci.* **2006**, *252*, 6513−6516.
(4) Mahoney, C. M.; Patwardhan, D. V.; McDermott, M. K. *Appl. Surf. Sci.* **2006**, *252*, 6554−6557.
(5) Mahoney, C. M.; Roberson, S.; Gillen, G. *Appl. Surf. Sci.* **2004**, *231*, 174−178.
(6) Mahoney, C. M.; Roberson, S. V.; Gillen, G. *Anal. Chem.* **2004**, *76*, 3199−3207.
(7) Mahoney, C. M.; Yu, J. X.; Fahey, A.; Gardella, J. A. *Appl. Surf. Sci.* **2006**, *252*, 6609−6614.
(8) Breitenstein, D.; Rommel, C. E.; Moellers, R.; Wegener, J.; Hagenhoff, B. *Angew. Chem., Int. Ed.* **2007**, *46*, 5332−5335.
(9) Breitenstein, D.; Rommel, C. E.; Stolwijk, J.; Wegener, J.; Hagenhoff, B. *Appl. Surf. Sci.* **2008**, *255*, 1249−1256.
(10) Fletcher, J. S.; Rabbani, S.; Henderson, A.; Lockyer, N. P.; Vickerman, J. C. *Rapid Commun. Mass Spectrom.* **2011**, *25*, 925−932.
(11) Ninomiya, S.; Ichiki, K.; Yamada, H.; Nakata, Y.; Seki, T.; Aoki, T.; Matsuo, J. *Rapid Commun. Mass Spectrom.* **2009**, *23*, 3264−3268.
(12) Cheng, J.; Wucher, A.; Winograd, N. *J. Phys. Chem. B* **2006**, *110*, 8329−8336.
(13) Shard, A. G.; Brewer, P. J.; Green, F. M.; Gilmore, I. S. *Surf. Interface Anal.* **2007**, *39*, 294−298.
(14) Sostarecz, A. G.; McQuaw, C. M.; Wucher, A.; Winograd, N. *Anal. Chem.* **2004**, *76*, 6651−6658.
(15) Krantzman, K. D.; Wucher, A. *J. Phys. Chem. C* **2010**, *114*, 5480−5490.
(16) Delcorte, A.; Garrison, B. J. *J. Phys. Chem. C* **2007**, *111*, 15312−15324.
(17) Mollers, R.; Tuccitto, N.; Torrisi, V.; Niehuis, E.; Licciardello, A. *Appl. Surf. Sci.* **2006**, *252*, 6509−6512.
(18) Mahoney, C. M.; Fahey, A. J.; Gillen, G.; Xu, C.; Batteas, J. D. *Appl. Surf. Sci.* **2006**, *252*, 6502−6505.
(19) Mahoney, C. M.; Fahey, A. J.; Gillen, G.; Xu, C.; Batteas, J. D. *Anal. Chem.* **2007**, *79*, 837−845.
(20) Sjovall, P.; Rading, D.; Ray, S.; Yang, L.; Shard, A. G. *J. Phys. Chem. B* **2010**, *114*, 769−774.
(21) Miyayama, T.; Sanada, N.; Iida, S. I.; Hammond, J. S.; Suzuki, M. *Appl. Surf. Sci.* **2008**, *255*, 951−953.
(22) Muramoto, S.; Brison, J.; Castner, D. G. *Anal. Chem.* **2012**, *84*, 365−372.
(23) Wagner, M. S. *Anal. Chem.* **2005**, *77*, 911−922.
(24) Lu, C. Y.; Wucher, A.; Winograd, N. *Anal. Chem.* **2011**, *83*, 351−358.
(25) Shard, A. G.; Green, F. M.; Brewer, P. J.; Seah, M. P.; Gilmore, I. S. *J. Phys. Chem. B* **2008**, *112*, 2596−2605.
(26) Paruch, R. J.; Postawa, Z.; Wucher, A.; Garrison, B. J. *J. Phys. Chem. C* **2012**, *116*, 1042−1051.
(27) Shard, A. G.; Foster, R.; Gilmore, I. S.; Lee, J. L. S.; Ray, S.; Yang, L. *Surf. Interface Anal.* **2011**, *43*, 510−513.

(28) Shard, A. G.; Ray, S.; Seah, M. P.; Yang, L. *Surf. Interface Anal.* **2011**, *43*, 1240−1250.
(29) Zalar, A. *Thin Solid Films* **1985**, *124*, 223−230.
(30) Iida, S.; Miyayama, T.; Sanada, N.; Suzuki, M.; Fisher, G. L.; Bryan, S. R. *e-J. Surf. Sci. Nanotechnol.* **2009**, *7*, 878−881.
(31) Kozole, J.; Willingham, D.; Winograd, N. *Appl. Surf. Sci.* **2008**, *255*, 1068−1070.
(32) Gillen, G.; Fahey, A.; Wagner, M.; Mahoney, C. *Appl. Surf. Sci.* **2006**, *252*, 6537−6541.
(33) Mao, D.; Wucher, A.; Winograd, N. *Anal. Chem.* **2010**, *82*, 57−60.
(34) Ninomiya, S.; Ichiki, K.; Yamada, H.; Nakata, Y.; Seki, T.; Aoki, T.; Matsuo, J. *Rapid Commun. Mass Spectrom.* **2009**, *23*, 1601−1606.
(35) Lee, J. L. S.; Ninomiya, S.; Matsuo, J.; Gilmore, I. S.; Seah, M. P.; Shard, A. G. *Anal. Chem.* **2010**, *82*, 98−105.
(36) Dowsett, M. G.; Rowlands, G.; Allen, P. N.; Barlow, R. D. *Surf. Interface Anal.* **1994**, *21*, 310−315.
(37) Brison, J.; Muramoto, S.; Castner, D. G. *J. Phys. Chem. C* **2010**, *114*, 5565−5573.
(38) Shard, A. G.; Seah, M. P. *Surf. Interface Anal.* **2011**, *43*, 1430−1435.
(39) Rabbani, S.; Barber, A. M.; Fletcher, J. S.; Lockyer, N. P.; Vickerman, J. C. *Anal. Chem.* **2011**, *83*, 3793−3800.
(40) Seki, T.; Murase, T.; Matsuo, J. *Nucl. Instrum. Methods Phys. Res. Sect. B* **2006**, *242*, 179−181.
(41) Gilmore, I. S.; Seah, M. P. *Appl. Surf. Sci.* **2003**, *203*, 600−604.
(42) Zheng, L. L.; Wucher, A.; Winograd, N. *Anal. Chem.* **2008**, *80*, 7363−7371.